# Fluctuating intertwined stripes in the strange metal regime of the Hubbard model

Edwin W. Huang,[1,*] Tianyi Liu,[2,3,*] Wen O. Wang,[2,4] Hong-Chen Jiang,[2] Peizhi Mai,[1] Thomas A. Maier,[5] Steven Johnston,[6,7] Brian Moritz,[2] and Thomas P. Devereaux[2,8,†]

[1]*Department of Physics and Institute of Condensed Matter Theory, University of Illinois at Urbana-Champaign, Urbana, Illinois 61801, USA*
[2]*Stanford Institute for Materials and Energy Sciences, SLAC National Accelerator Laboratory, 2575 Sand Hill Road, Menlo Park, California 94025, USA*
[3]*Department of Chemistry, Stanford University, Stanford, California 94305, USA*
[4]*Department of Applied Physics, Stanford University, Stanford, California 94305, USA*
[5]*Computational Sciences and Engineering Division, Oak Ridge National Laboratory, Oak Ridge, Tennessee, 37831-6494, USA*
[6]*Department of Physics and Astronomy, The University of Tennessee, Knoxville, Tennessee 37996, USA*
[7]*Institute of Advanced Materials and Manufacturing, The University of Tennessee, Knoxville, Tennessee 37996, USA*
[8]*Department of Materials Science and Engineering, Stanford University, Stanford, California 94305, USA*

(Received 13 December 2022; revised 26 January 2023; accepted 30 January 2023; published 15 February 2023)

Strongly correlated electron systems host a variety of poorly understood correlations in their high-temperature normal state. Unlike ordered phases defined by order parameters, regions of the normal state are often defined through unconventional properties such as strange metallic transport or spectroscopic pseudogaps. Characterizing the microscopic correlations in the normal state is necessary to elucidate mechanisms that lead to these properties and their connection to ground-state orders. Here we establish the presence of intertwined charge and spin stripes in the strange metal normal state of the Hubbard model using determinant quantum Monte Carlo calculations. The charge and spin density waves constituting the stripes are fluctuating and short ranged; yet they obey a mutual commensurability relation and remain microscopically interlocked, as evidenced through measurements of three-point spin-spin-hole correlation functions. Our findings demonstrate the ability of many-body numerical simulations to unravel the microscopic correlations that define quantum states of matter.

DOI: 10.1103/PhysRevB.107.085126

The concept of intertwined orders is commonly used to characterize states within the pseudogap regime of the cuprate phase diagram [1,2]. A well-known example is that of stripe order, unidirectional spin and charge density waves that are most prominent at low temperatures around $p = 1/8$ hole doping [3–6]. In La-based cuprates [7,8] and in simulations of the Hubbard model [5], spin and charge stripes are interlocked. Regions of high hole concentration are aligned with antiferromagnetic phase reversals. Stripe order is well known to interact closely with superconductivity, as evidenced by 1/8 anomalies in cuprate experiments [9] and by nearly degenerate ground-state energies in Hubbard model calculations [5,10]. The close interplay of spin and charge orders and their competition with superconductivity are believed to be hallmarks of the pseudogap regime.

The majority of recent progress in solving the Hubbard model has targeted ground-state properties [11–17]. Studies at finite temperature have found fluctuating spin and charge stripes [6,18,19], but their interplay, doping dependence, and placement in the broader phase diagram have not been explored thoroughly. Our calculations of the Hubbard model demonstrate interlocked spin and charge stripes at temperatures above the onset of the pseudogap, in the strange metal regime characterized by $T$-linear resistivity [20,21]. The wide range of doping where we find stripes corroborates a growing number of experimental studies finding charge stripes in optimally doped and overdoped cuprates [22–30].

Our results are based on unbiased determinant quantum Monte Carlo (DQMC) simulations [31,32] conducted with very large sample sizes. Typical simulations involve $\sim 10^{10}$ measurements, allowing for small stochastic errors ($\sim 10^{-6}$) despite the presence of a fermion sign problem. The principal observables we compute to investigate stripes in the Hubbard model are the charge and spin susceptibilities at zero frequency, defined as

$$\chi_c(\mathbf{r}) = \int_0^\beta d\tau \langle n_{\mathbf{r}}(\tau) n_{\mathbf{0}} \rangle - \langle n_{\mathbf{r}} \rangle \langle n_{\mathbf{0}} \rangle, \tag{1}$$

$$\chi_s(\mathbf{r}) = \int_0^\beta d\tau \left\langle m^z_{\mathbf{r}}(\tau) m^z_{\mathbf{0}} \right\rangle, \tag{2}$$

where $n_{\mathbf{r}} = n_{\mathbf{r}\uparrow} + n_{\mathbf{r}\downarrow}$ and $m^z_{\mathbf{r}} = \frac{1}{2}(n_{\mathbf{r}\uparrow} - n_{\mathbf{r}\downarrow})$ are the charge and spin densities on site $\mathbf{r}$. These quantities can be computed directly with DQMC, without the need for analytic continuation, so that our results are numerically exact.

Figure 1(a) displays the spin and charge susceptibilities as functions of $\mathbf{r}$ for a $12 \times 4$ rectangular cluster with periodic boundary conditions at doping $p = 1/8$. The spin susceptibility is plotted with a staggering factor $[\chi_s^*(\mathbf{r}) = \chi_s(\mathbf{r}) \times (-1)^{r_x + r_y}]$ to highlight deviations from commensurate anti-

*These authors contributed equally to this work.
†tpd@stanford.edu

 

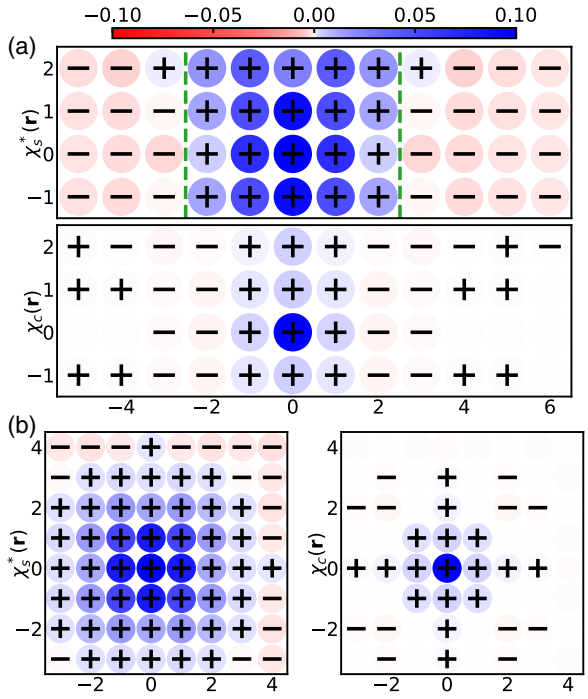


FIG. 1. Stripes in spin and charge susceptibilities. (a) and (b) Spin susceptibility $\chi_s(\mathbf{r})$ and charge susceptibility $\chi_c(\mathbf{r})$ at zero frequency in the Hubbard model. The spin susceptibility is plotted with a staggering factor for clarity [$\chi_s^*(\mathbf{r}) = \chi_s(\mathbf{r}) \times (-1)^{r_x+r_y}$]. Parameters are $U/t = 6, t'/t = -0.25, T/t \approx 0.22, p = 0.125$. Cluster size is (a) $12 \times 4$ and (b) $8 \times 8$. + and − signs indicate correlations that are nonzero by at least two standard errors. Green dashed lines in (a) denote the antiphase domain walls of spin stripes. The diamond patterns of modulation in (b) indicate a superposition of stripes along $x$ and $y$ directions.

ferromagnetism. In both the spin and charge susceptibilities, periodic modulations are visible along the long direction of the cluster, indicating the presence of short-ranged fluctuating stripes. The charge modulation has a shorter correlation length and a period that is approximately half of that of the spin modulation, consistent with a stripe pattern where antiphase domain walls in the spin density coincide with regions of increased hole density [33,34]. The pattern of modulation in the spin susceptibility is identical to that in the equal-time ($\tau = 0$) spin correlation function (Figs. S1 and S2), analyzed previously in Ref. [6]. By contrast, the stripe modulations in the charge susceptibility are not visible in the equal-time charge correlation function [19], at the temperatures attainable in our simulations. This distinction is related to the fact that high-energy incoherent excitations contaminate the equal-time correlation function more than the static susceptibility, as emphasized in Ref. [3].

We have checked that the finite-size cluster does not have a notable impact on the properties of the stripe pattern (Figs. S1–S3). We focus on $12 \times 4$ cluster results in Figs. 1(a) and 2 as the larger average fermion sign associated with smaller cluster size enables us to more clearly resolve modulations in the charge susceptibility. We consider an $8 \times 8$ cluster in Fig. 1(b). Here, modulations are again visible in both the spin and charge susceptibilities, with negative regions along the diagonal directions. This pattern is precisely expected from a superposition of horizontal and vertical stripes. Our analysis indicates that the stripe modulations seen for the $12 \times 4$ cluster are not artifacts of limited system size. The doping dependence of the spin and charge susceptibilities is shown in Fig. 2. In Figs. 2(a)–2(c), we plot the susceptibilities for hole doping concentrations of $p = 0.1$, 0.15, and 0.2. Modulations are present, indicating fluctuating spin and charge stripes for all three doping levels. The period of the modulation decreases with increased hole doping. This is also clearly reflected in momentum-space susceptibilities. In Fig. 2(d), the spin susceptibility splits from a single peak at $(\pi, \pi)$ [i.e., (0.5, 0.5) in reciprocal lattice units] to two incommensurate peaks with increased hole doping. The data are well fit with periodic Lorentzian functions (see Supplemental Material Sec. C [35]). Similarly, the charge susceptibility [Fig. 2(e)] splits away from $\mathbf{q} = (0, 0)$ as hole doping increases and rises uniformly owing to the increased metallicity of the doped system. For hole doping $0.1 \leqslant p \leqslant 0.2$ we obtain excellent fits to $\chi_c(\mathbf{q})$ with periodic Lorentzian functions plus a constant background. In Fig. S5(b), we check that the charge susceptibilities are indeed peaked close to (0,0) or $(\pi, 0)$, rather than near $(\pi, \pi)$ as in the noninteracting model. This indicates that the fluctuating stripes we observe are unrelated to Fermi surface effects such as nesting and cannot be captured by weak-coupling approaches such as the random phase approximation (RPA).

From our fits to $\chi_s(\mathbf{q})$ and $\chi_c(\mathbf{q})$, we extract the spin and charge incommensurabilities, defined as the separation of the incommensurate peaks from the commensurate wave vectors [(0,0) for charge and $(\pi, \pi)$ for spin]. Figure 2(f) plots the spin and charge incommensurabilities against doping. The spin incommensurability is very close to half the charge incommensurability through the range of doping $0.1 \leqslant p \leqslant 0.2$, indicating that the stripes are mutually commensurate. Both increase monotonically with hole doping, with a stripe filling in between half filled (dashed line) and fully filled (dotted line).

The mutual commensurability of the spin and charge stripes strongly suggests, but does not prove, that doped holes reside near antiphase domain walls. It is known that modifying the chemical potential on a column can pin the location of antiphase domain walls [36], and conversely that including a staggered magnetic field on a column can induce a static charge stripe modulation [19]. However, whether spin and charge stripes are pinned to each other while still fluctuating is unknown. To resolve this question and probe the relation between fluctuating spin and charge stripes, we consider the 3-point spin-spin-hole correlation function

$$\left\langle m^z_{\mathbf{r}} m^z_{\mathbf{0}} h_{\mathbf{r}'} \right\rangle, \tag{3}$$

where $h_{\mathbf{r}'} = c_{\mathbf{r}'\uparrow} c^\dagger_{\mathbf{r}'\uparrow} c_{\mathbf{r}'\downarrow} c^\dagger_{\mathbf{r}'\downarrow}$ ensures the presence of a hole on site $\mathbf{r}'$. In Fig. 3(a) we first plot $\langle m^z_{\mathbf{r}} m^z_{\mathbf{0}} \rangle \langle h_{\mathbf{r}'} \rangle$ to demonstrate how the 3-point correlation function would appear if spin and charge were entirely decoupled. By translation symmetry, $\langle h_{\mathbf{r}'} \rangle$ is a constant, and Fig. 3(a) thus simply shows the spin correlation function. Figure 3(b) shows the full 3-point correlation function, with the axes and letter "h" indicating

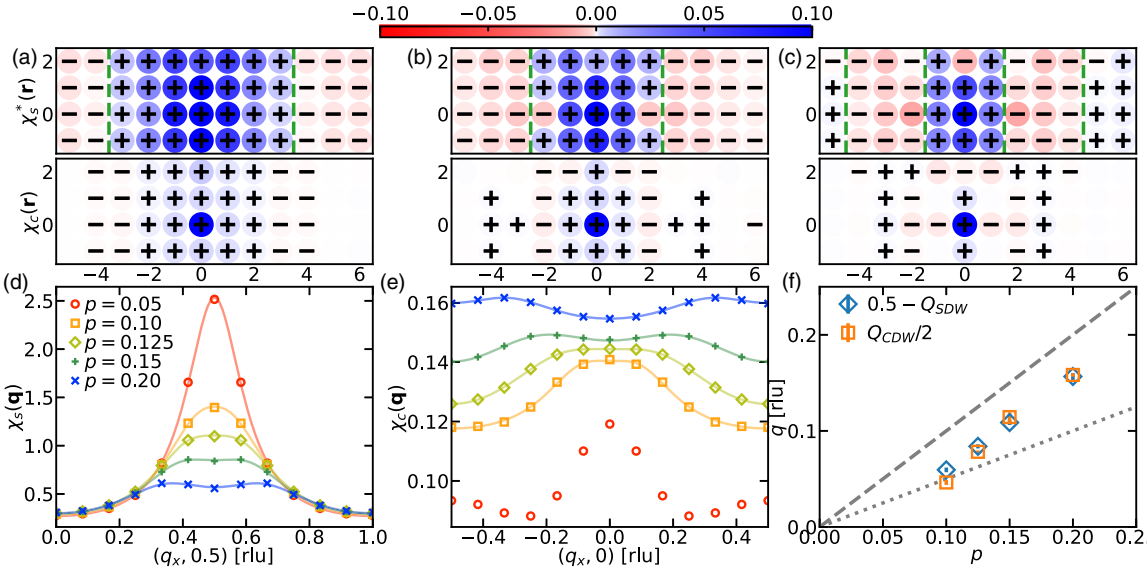


FIG. 2. Doping dependence of spin and charge stripes. (a), (b), and (c) Staggered spin susceptibilities and charge susceptibilities for dopings 0.1, 0.15, and 0.2, respectively, on a $12 \times 4$ cluster with parameters $U/t = 6, t'/t = -0.25, T/t \approx 0.22$. (d) and (e) Momentum-space susceptibilities for spin and charge, respectively, for various doping concentrations. Solid lines indicate fits to periodic Lorentzian functions (see Supplemental Material Sec. C [35]). No stripes are present at $p = 0.05$, and the Lorentzian fit to $\chi_c(\mathbf{q})$ is poor and not shown. (f) Spin and charge incommensurabilities as a function of doping, obtained from fits to the momentum-space susceptibilities. Dashed and dotted lines indicate $q = p$ and $q = p/2$, corresponding to the spin incommensurabilities of half-filled and filled stripes, respectively. CDW, charge density wave; SDW, spin density wave; rlu, reciprocal lattice units.

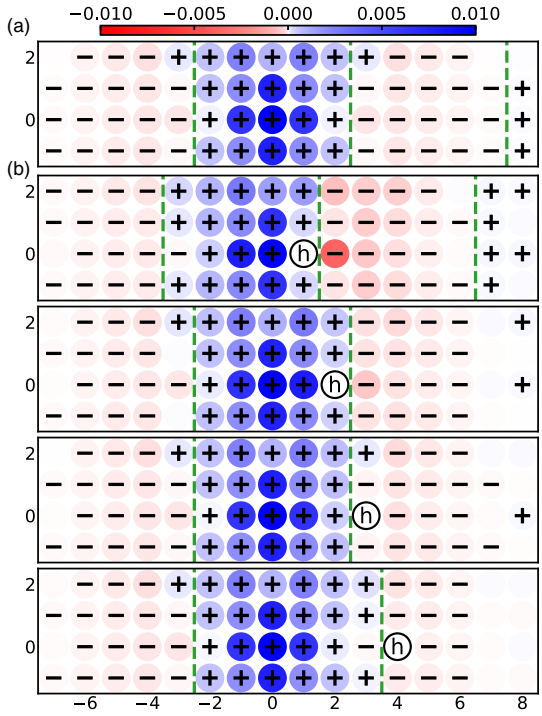


FIG. 3. Holes pin antiphase domain walls. (a) Uncorrelated value $\langle m^z_{\mathbf{r}} m^z_{\mathbf{0}} \rangle \langle h_{\mathbf{r}'} \rangle$ demonstrating expectations if spin and charge were decoupled. As in Figs. 1 and 2, a staggering factor $(-1)^{r_x + r_y}$ is included for clarity. (b) Full spin-spin-hole correlation function $\langle m^z_{\mathbf{r}} m^z_{\mathbf{0}} h_{\mathbf{r}'} \rangle$ indicating spin correlations in the presence of a hole. The location of the hole on $\mathbf{r}'$ is indicated by the letter "h." The antiphase domain walls (green dashed lines) move as $\mathbf{r}'$ is varied. Parameters are $U/t = 6, t'/t = -0.25, p = 0.125, T/t = 0.22$. Additional plots for other locations of the hole may be found in Fig. S8.

the coordinates of $\mathbf{r}$ and $\mathbf{r}'$, respectively. In these 3-point correlation functions, it is clear that while the periodicity of spin stripes is unaffected, there is a strong tendency for the antiphase domain walls to lie adjacent to the hole. This establishes definitively that although both the spin and charge stripes seen in Figs. 1 and 2 are short ranged and fluctuating, they remain microscopically interlocked. This close interplay between fluctuating spin and charge stripes in our finite-temperature calculations indicates that the notion of intertwined orders is not unique to the pseudogap regime of the phase diagram.

In the data presented thus far, we have focused on results at a temperature $T/t \approx 0.22$, near the lowest accessible in our simulations due to the fermion sign problem. In Fig. 4, we discuss the evolution of the strength of the fluctuating stripes with temperature and doping. We consider the value of the spin and charge susceptibilities at the nearest vertical neighbor, $\chi_s(\mathbf{r} = \hat{y})$ and $\chi_c(\mathbf{r} = \hat{y})$, as simple estimates of the magnitude of the fluctuating stripes (see Supplemental Material Sec. A 5 [35]). The doping and temperature dependence of $\chi_{c,s}(\mathbf{r} = \hat{y})$ is plotted in Fig. 4(a). For doping concentrations or temperatures where $\chi_c(\mathbf{r} = \hat{y}) < 0$, the patterns in the charge susceptibility do not resemble stripes (Fig. S6). We observe that the spin stripes weaken monotonically with increasing doping and increasing temperature, but the charge stripes display a nonmonotonic doping dependence with a maximum at $p = 1/8$. This peak is highly reminiscent of $1/8$ anomalies in cuprate superconductors, where charge stripes have also been observed to have maximal strength at $p = 1/8$, with a concomitant suppression of superconductivity. The broad peak at $p = 1/8$ is also reminiscent of a similar peak seen in a $\mathbf{q} = 0$ nematic susceptibility reported previously for the Hubbard model [37].

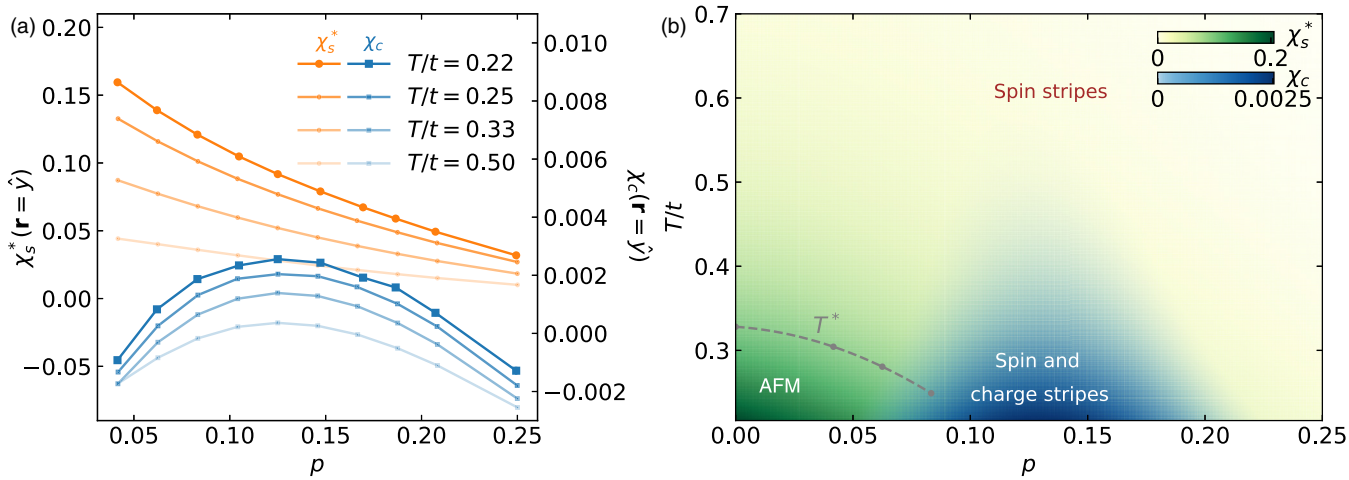


FIG. 4. Doping and temperature dependence of stripe intensity. (a) Staggered spin $[\chi_s^*(\boldsymbol{r} = \hat{y})]$ and charge $[\chi_c(\boldsymbol{r} = \hat{y})]$ susceptibilities at the $y$ neighbor, as a function of doping for different temperatures. Lines are guides to the eye. (b) Schematic temperature-doping phase diagram drawn using data from (a). The yellow-green background corresponds to $\chi_s^*(\hat{y})$, indicating local antiferromagnetic (AFM) correlations throughout the temperature doping ranges. Darker colors indicate larger magnitude. The blue region indicates positive $\chi_c(\hat{y})$, and the color intensity corresponds to the value of the susceptibility. Cubic spline interpolation is applied to data points in the temperature-doping grid to obtain smoothly varying color intensity. The dashed gray line indicates the approximate crossover temperatures of the pseudogap regime, $T^*$, estimated by locating the temperatures that maximize the spin (Pauli) susceptibilities or Knight shift for various dopings (Fig. S7).

Both spin and charge stripes grow in intensity as temperature decreases. While there is no sharp definition for the onset temperature of fluctuating stripes, given their short-ranged nature, we generally find that modulations indicative of charge stripes have their onset at lower temperatures than spin stripes. Our findings are summarized in a temperature-doping "phase diagram" in Fig. 4(b), where the color intensity corresponds to the magnitude of $\chi_s(\mathbf{r} = \hat{y})$ in the yellow-green background, on top of which a blue region around $p = 1/8$ corresponding to $\chi_c(\mathbf{r} = \hat{y})$ is overlaid. In general, we find that incommensurate spin correlations indicative of spin stripes become visible below roughly $T/t \approx 0.6$. Charge stripes become visible at lower temperatures, for instance, $T/t \approx 0.5$ at $p = 1/8$ (see Supplemental Material Sec. D [35] and Refs. [6,19,38]).

We emphasize that the clear and robust signatures of interlocked spin and charge stripes occur at temperatures well above the onset of the pseudogap. The pseudogap crossover temperature $T^*$ is estimated by the peak in the Knight shift $\chi_s(\mathbf{q} = 0, \omega = 0)$ as a function of temperature (see Supplemental Material Sec. E [35]). $T^*$ for different doping is plotted in Fig. 4(b). As $T^*$ decreases with increased hole doping, we cannot explore the behavior of fluctuating stripes below the pseudogap onset temperature within unbiased DQMC simulations. Nevertheless, we find strong signatures of fluctuating spin and charge stripes over a significant range of hole doping, thus demonstrating that the pseudogap is not a prerequisite for intertwined orders. In fact, the temperatures and doping levels at which our simulations are conducted lie in the strange metal regime of the phase diagram, as supported by previous DQMC calculations of the Hubbard model finding large, $T$-linear resistivity [21]. Our findings motivate further studies and analysis of theories connecting fluctuating stripes to strange metallic transport [39–42].

The presence of stripes in the strange metal regime is further substantiated by a number of recent x-ray scattering experiments finding scattering from fluctuating charge density waves in optimally and overdoped cuprate compounds at temperatures approaching room temperature [22–29]. A recent detailed analysis of $La_{1.8-x}Eu_{0.2}Sr_xCuO_4$ (Eu-LSCO) [29] showed a nearly temperature-independent integrated intensity of the charge scattering peak over range of doping $0.1 \leqslant p \leqslant 0.2$, indicating that the amplitude of the charge order has its onset above experimentally accessible temperatures and that stripes persist well into the strange metal. Interestingly, the same study suggests decoupling of spin and charge stripes at elevated temperatures, with a charge ordering wave vector that decreases with increasing doping, highly reminiscent of the behavior of Y- and Bi-based cuprates. These differences are not captured in the Hubbard model and point toward the importance of effects beyond the local Hubbard interaction, including electron-phonon coupling, long-range Coulomb interactions, and effects of the oxygen orbitals that are not fully contained in a single-band model. Nevertheless, the concordance of our numerical results on the simplified Hubbard model and recent experimental works [22–30] finding stripes beyond the pseudogap regime highlights the importance of fluctuating stripes over a larger region of the phase diagram than previously considered. Their existence over wide ranges of doping and temperature is evidence of their relevance to all electronic properties of cuprates. Our findings call for further investigations of intertwined order in other strongly correlated materials and strange metals.

The data that support the findings of this study are available from the corresponding author upon reasonable request.

The work at Stanford and SLAC (T.L., W.O.W., H.-C.J., B.M., and T.P.D.) was supported by the U.S. Department of Energy (DOE), Office of Basic Energy Sciences, Materials Sciences and Engineering Division, under Contract No. DE-AC02-76SF00515. E.W.H. was supported by the Gordon and Betty Moore Foundation EPiQS Initiative through GBMF

Grants No. 4305 and No. 8691. P.M. acknowledges support from Center for Emergent Superconductivity, a DOE Energy Frontier Research Center, Grant No. DE-AC0298CH1088. Work by S.J. and T.A.M. was supported by the U.S. Department of Energy, Office of Science, Office of Basic Energy Sciences, under Award No. DE-SC0022311. Computational work was performed on the Sherlock cluster at Stanford University and on resources of the National Energy Research Scientific Computing Center, supported by the U.S. Department of Energy under Contract No. DE-AC02-05CH11231.

E.W.H., T.L., and W.O.W. performed DQMC simulations. E.W.H. and T.L. analyzed the data. T.P.D. and B.M. supervised the project. All authors discussed the results and participated in writing the manuscript.

The authors declare no competing financial or nonfinancial interests.

[1] E. Fradkin and S. A. Kivelson, Nat. Phys. **8**, 864 (2012).
[2] E. Fradkin, S. A. Kivelson, and J. M. Tranquada, Rev. Mod. Phys. **87**, 457 (2015).
[3] S. A. Kivelson, I. P. Bindloss, E. Fradkin, V. Oganesyan, J. M. Tranquada, A. Kapitulnik, and C. Howald, Rev. Mod. Phys. **75**, 1201 (2003).
[4] E. W. Huang, C. B. Mendl, S. Liu, S. Johnston, H.-C. Jiang, B. Moritz, and T. P. Devereaux, Science **358**, 1161 (2017).
[5] B.-X. Zheng, C.-M. Chung, P. Corboz, G. Ehlers, M.-P. Qin, R. M. Noack, H. Shi, S. R. White, S. Zhang, and G. K.-L. Chan, Science **358**, 1155 (2017).
[6] E. W. Huang, C. B. Mendl, H.-C. Jiang, B. Moritz, and T. P. Devereaux, npj Quantum Mater. **3**, 22 (2018).
[7] J. M. Tranquada, B. J. Sternlieb, J. D. Axe, Y. Nakamura, and S. Uchida, Nature (London) **375**, 561 (1995).
[8] J. M. Tranquada, M. P. M. Dean, and Q. Li, J. Phys. Soc. Jpn. **90**, 111002 (2021).
[9] D. Feng, Z.-X. Shen, X. Zhou, K. Shen, D. Lu, and D. Marel, J. Phys. Chem. Solids **67**, 198 (2006).
[10] P. Corboz, T. M. Rice, and M. Troyer, Phys. Rev. Lett. **113**, 046402 (2014).
[11] D. P. Arovas, E. Berg, S. A. Kivelson, and S. Raghu, Annu. Rev. Condens. Matter Phys. **13**, 239 (2022).
[12] M. Qin, T. Schäfer, S. Andergassen, P. Corboz, and E. Gull, Annu. Rev. Condens. Matter Phys. **13**, 275 (2022).
[13] H.-C. Jiang and T. P. Devereaux, Science **365**, 1424 (2019).
[14] M. Qin, C.-M. Chung, H. Shi, E. Vitali, C. Hubig, U. Schollwöck, S. R. White, and S. Zhang (Simons Collaboration on the Many-Electron Problem), Phys. Rev. X **10**, 031016 (2020).
[15] C.-M. Chung, M. Qin, S. Zhang, U. Schollwöck, and S. R. White (The Simons Collaboration on the Many-Electron Problem), Phys. Rev. B **102**, 041106(R) (2020).
[16] Y.-F. Jiang, J. Zaanen, T. P. Devereaux, and H.-C. Jiang, Phys. Rev. Res. **2**, 033073 (2020).
[17] S. Sorella, arXiv:2101.07045 [cond-mat.str-el].
[18] A. Wietek, Y.-Y. He, S. R. White, A. Georges, and E. M. Stoudenmire, Phys. Rev. X **11**, 031007 (2021).
[19] P. Mai, S. Karakuzu, G. Balduzzi, S. Johnston, and T. A. Maier, Proc. Natl. Acad. Sci. USA **119**, e2112806119 (2022).
[20] P. T. Brown, D. Mitra, E. Guardado-Sanchez, R. Nourafkan, A. Reymbaut, C.-D. Hébert, S. Bergeron, A.-M. S. Tremblay, J. Kokalj, D. A. Huse, P. Schauß, and W. S. Bakr, Science **363**, 379 (2019).
[21] E. W. Huang, R. Sheppard, B. Moritz, and T. P. Devereaux, Science **366**, 987 (2019).
[22] R. Arpaia, S. Caprara, R. Fumagalli, G. D. Vecchi, Y. Y. Peng, E. Andersson, D. Betto, G. M. D. Luca, N. B. Brookes, F. Lombardi, M. Salluzzo, L. Braicovich, C. D. Castro, M. Grilli, and G. Ghiringhelli, Science **365**, 906 (2019).
[23] H. Miao, G. Fabbris, R. J. Koch, D. G. Mazzone, C. S. Nelson, R. Acevedo-Esteves, G. D. Gu, Y. Li, T. Yilimaz, K. Kaznatcheev, E. Vescovo, M. Oda, T. Kurosawa, N. Momono, T. Assefa, I. K. Robinson, E. S. Bozin, J. M. Tranquada, P. D. Johnson, and M. P. M. Dean, npj Quantum Mater. **6**, 31 (2021).
[24] J. Q. Lin, H. Miao, D. G. Mazzone, G. D. Gu, A. Nag, A. C. Walters, M. García-Fernández, A. Barbour, J. Pelliciari, I. Jarrige, M. Oda, K. Kurosawa, N. Momono, K.-J. Zhou, V. Bisogni, X. Liu, and M. P. M. Dean, Phys. Rev. Lett. **124**, 207005 (2020).
[25] Y. Y. Peng, R. Fumagalli, Y. Ding, M. Minola, S. Caprara, D. Betto, M. Bluschke, G. M. De Luca, K. Kummer, E. Lefrançois, M. Salluzzo, H. Suzuki, M. Le Tacon, X. J. Zhou, N. B. Brookes, B. Keimer, L. Braicovich, M. Grilli, and G. Ghiringhelli, Nat. Mater. **17**, 697 (2018).
[26] W. S. Lee, K.-J. Zhou, M. Hepting, J. Li, A. Nag, A. C. Walters, M. Garcia-Fernandez, H. C. Robarts, M. Hashimoto, H. Lu, B. Nosarzewski, D. Song, H. Eisaki, Z. X. Shen, B. Moritz, J. Zaanen, and T. P. Devereaux, Nat. Phys. **17**, 53 (2021); **17**, 659(E) (2021).
[27] Q. Ma, K. C. Rule, Z. W. Cronkwright, M. Dragomir, G. Mitchell, E. M. Smith, S. Chi, A. I. Kolesnikov, M. B. Stone, and B. D. Gaulin, Phys. Rev. Res. **3**, 023151 (2021).
[28] C. C. Tam, M. Zhu, J. Ayres, K. Kummer, F. Yakhou-Harris, J. R. Cooper, A. Carrington, and S. M. Hayden, Nat. Commun. **13**, 570 (2022).
[29] S. Lee, E. W. Huang, T. A. Johnson, X. Guo, A. A. Husain, M. Mitrano, K. Lu, A. V. Zakrzewski, G. A. de la Peña, Y. Peng, H. Huang, S.-J. Lee, H. Jang, J.-S. Lee, Y. I. Joe, W. B. Doriese, P. Szypryt, D. S. Swetz, S. Chi, A. A. Aczel *et al.*, Proc. Natl. Acad. Sci. USA **119**, e2119429119 (2022).
[30] S. Kawasaki, M. Ito, D. Kamijima, C. Lin, and G.-q. Zheng, J. Phys. Soc. Jpn. **90**, 111008 (2021).
[31] S. R. White, D. J. Scalapino, R. L. Sugar, E. Y. Loh, J. E. Gubernatis, and R. T. Scalettar, Phys. Rev. B **40**, 506 (1989).
[32] R. Blankenbecler, D. J. Scalapino, and R. L. Sugar, Phys. Rev. D **24**, 2278 (1981).
[33] J. Zaanen and O. Gunnarsson, Phys. Rev. B **40**, 7391 (1989).
[34] J. Zaanen, O. Y. Osman, H. V. Kruis, Z. Nussinov, and J. Tworzydlo, Philos. Mag. B **81**, 1485 (2001).
[35] See Supplemental Material at http://link.aps.org/supplemental/10.1103/PhysRevB.107.085126 for DQMC methodology, finite-size analysis, description of the susceptibility fitting,

temperature dependence of stripes, and analysis of the pseudogap crossover temperature.

[36] R. Mondaini, T. Ying, T. Paiva, and R. T. Scalettar, Phys. Rev. B **86**, 184506 (2012).

[37] T. Liu, D. Jost, B. Moritz, E. W. Huang, R. Hackl, and T. P. Devereaux, Phys. Rev. B **103**, 134502 (2021).

[38] M. Fujita, H. Goka, K. Yamada, J. M. Tranquada, and L. P. Regnault, Phys. Rev. B **70**, 104517 (2004).

[39] L. V. Delacrétaz, B. Goutéraux, S. A. Hartnoll, and A. Karlsson, SciPost Phys. **3**, 025 (2017).

[40] L. V. Delacrétaz, B. Goutéraux, S. A. Hartnoll, and A. Karlsson, Phys. Rev. B **96**, 195128 (2017).

[41] T. Andrade, A. Krikun, K. Schalm, and J. Zaanen, Nat. Phys. **14**, 1049 (2018).

[42] S. Caprara, C. D. Castro, G. Mirarchi, G. Seibold, and M. Grilli, Commun. Phys. **5**, 10 (2022).